Implementation of dual stripmap imaging for a novel airborne SAR system

JIN Xuesong, LI Yong

College of Information Science and Technology, *Nanjing University of Aeronautics and Astronautics*, *Jiangsu Nanjing* 210016, *China*

Abstract: This paper studies the dual stripmap imaging program of the airborne SAR which carries a circular scanning antenna system that has the ability to map both sides of the radar's flight path. This imaging mode is developed from the circular-scanning mode, which effectively improves the image size and the imaging efficiency. The basic imaging procedure is firstly analyzed, then the implementation as well as the rules of choosing the system parameters to fulfill the image resolution and the seamless mosaicing requirements are presented, while considering the actual motion conditions of the radar platform. The point-target simulation and live data processing results of one real system are given to show the validity of the proposed imaging methodology.

Key words: synthetic aperture radar (SAR), dual stripmap mode, imaging algorithm, parameter design

CLC number: TP722.6 **Document code:** A

Citation format: Jin X S and Li Y. 2010. Implementation of dual stripmap imaging for a novel airborne SAR system. *Journal of Remote Sensing*. **14**(4): 681—693

1 INTRODUCTION

Synthetic aperture radar (SAR) with the capabilities of all-weather, day and night, and long distance imaging, is widely used in the Earth′s surface mapping, resource exploration and other fields. Achieving multi-mode high-resolution imaging is one of SAR development directions. In the classic stripmap mode, the spotlight mode and the scanning mode (Ian & Frank, 2007; Carrara & Goodman, 1995), the imaging area locates on the single side of radar flight path. For the circular-scanning SAR (Li *et al*., 2008; Li *et al*., 2002) (Fig.1), the both side of the flight path can be illuminated synchronously by steering the radar antenna to rotate continuously around with the vertical axes pointing to the Earth surface. However, the circular-scanning SAR system does have insuperable disadvantages. Firstly, with the scanning of radar beam, the increasing of squint angle leads to a lower utilization rate of synthetic aperture and thus a lower azimuth resolution. Secondly, the image formation becomes difficult where the beam pointing the forward or backward directions due to the serious coupling of the range and azimuthal signals (Mao *et al*., 2008). Therefore, the effective information of circular-scanning SAR image is mostly concentrated at the broad sides of stripmap. The focused processing where the radar beam pointing to the forward or backward not only costs actra hardware resources and computing time, but also can not provide us the desirable results.

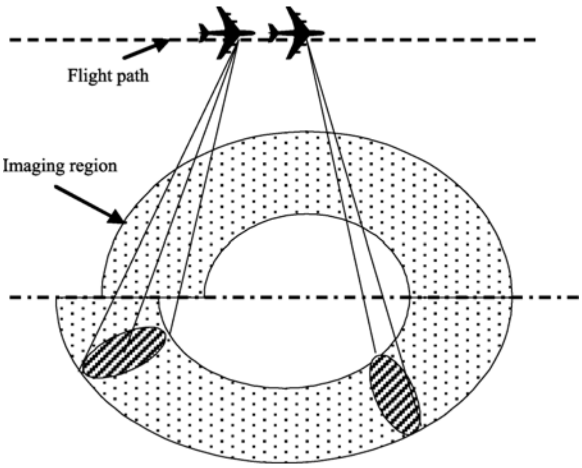

Fig. 1 Sketch map of circular scanning SAR

Thus, one kind of dual stripmap SAR imaging algorithm is studied in this paper (Fig.2). This model is based on circular-scanning SAR system, which satisfies wide imaging area and high resolution requirements as well as the improved imaging efficiency. By introducing additional geometric correction and image mosaic prosessing, it can achieve some new capabilities rather than other systems. The model makes up for the shortage of single stripmap SAR in some special stations. It may improve the guidance precision of all kinds of airborne weapons combined with a circular-scanning SAR. In this paper,

Received: 2009-06-05; **Accepted**: 2009-11-03

Foundation: Aeronautical Science Foundation of China (No. 20080152004) and Ph.D. Programs Foundation of Ministry of Education of China (No. 20070287053).

First author biography: JIN Xuesong (1985—), male, master of engineering. He majors in radar signal processing. E-mail: xuesong.jin@163.com

the implementation steps and the design requirements of the system parameters for dual stripmap SAR imaging are analyzed detailedly. Finally, the simulation and live data processing results are given to verify the validity of the imaging algorithm.

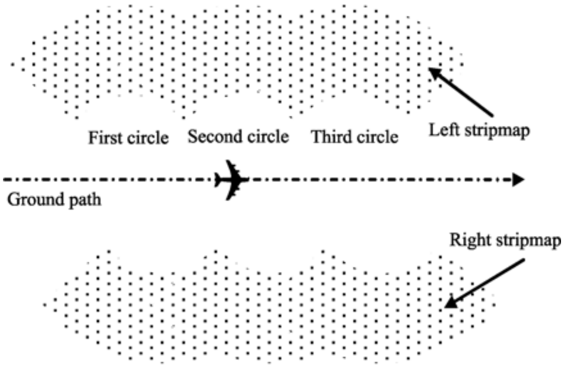

Fig. 2 Sketch map of dual stripmap SAR

2 ANALYSIS OF DUAL STRIPMAP IMAGING ALGORITHM

The processing block diagram of dual stripmap SAR imaging is shown in Fig.3. As the platform moves, the radar antenna system transmits signals while rotating with the vertical axis with the same inclination angle, and then receives the echo. The system processes the echo from both sides of platform and then produces the subimages. Subimages are mosaicked after geometric distortion correction into the sector image during the circular scanning period. With the sector image generated and mosaicked unceasingly, dual stripmap image is obtained.

2.1 Imaging geometry model

It is convenient for the following discussion by define t=0 when the radar beam points to the scene center (Point O), which along with the instantaneous squint angel ε in the slant plane and $\theta_r(t)$ in XOY determines the aperture center (Point C) of the antenna phase center (APC).

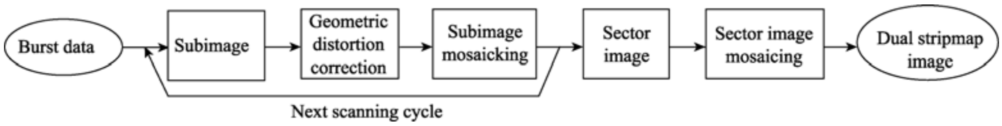

Fig. 3 Processing block diagram of dual stripmap SAR Imaging

As depicted in Fig.4, the radar antenna rotates at a constant rate by Ω_M. Provided that β_a and β_r is the two-way azimuth and range beamwidth respectively. The size of radar antenna footprint denoted approximately as the circular sector can be calculated as

$$\begin{cases} r_0 = H\tan\phi \\ r_1 = H\tan(\phi - \dfrac{\beta_r}{2}) \\ r_2 = H\tan(\phi + \dfrac{\beta_r}{2}) \\ \varphi_a \approx \dfrac{\beta_a}{\sin\phi} \end{cases} \tag{1}$$

where H is the flying height, ϕ is the incidence angle, φ_a is the center angle of the sector, r_0 is the central radius, r_1 and r_2 is respectively the lower and upper limit radius. Furthermore, the 3-D instantaneous position of the APC, i.e.[$x(t)$, $y(t)$, $z(t)$], is expressed as

$$\begin{cases} x(t) = x(0) - v_x t \\ y(t) = y(0) \\ z(t) = H \end{cases} \tag{2}$$

where t is the slow time in azimuth, [$x(0)$, $y(0)$, H] is the 3-D position of the APC at the aperture center C. The 3-D instantaneous position of the point O, i.e. [$x_{of}(t)$, $y_{of}(t)$, $z_{of}(t)$], is expressed as

$$\begin{cases} x_{of}(t) = x(t) + r_0\cos\theta(t) \\ y_{of}(t) = y(t) + r_0\sin\theta(t) \\ z_{of}(t) = 0 \end{cases} \tag{3}$$

where $\theta_r(t)$=θ_0−$\Omega_M t$ is the instantaneous scanning angle of radar antenna.

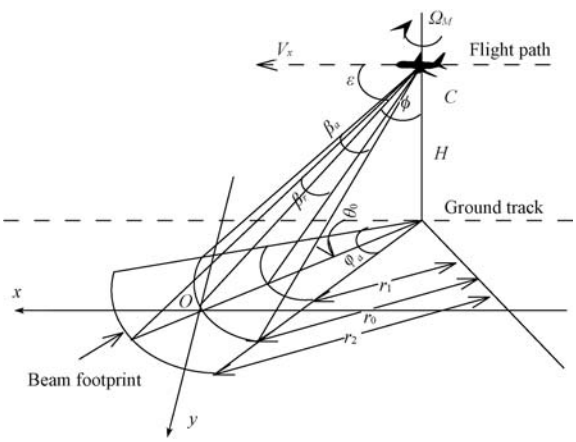

Fig. 4 Circular-scanning SAR data collecting geometry

2.2 Subimage imaging

In this paper, the linear range Doppler (LRD) algorithm is used, which meets the imaging requirements in high squint mode and large flexibility of radar platform. LRD algorithm is based on turntable imaging principle. Due to real-time and low computational complexity, it is suitable for engineering application.

The transmitted signal by the radar is

$$p(\tau) = m(\tau)\cos\left[2\pi\frac{c}{\lambda}\tau + \pi\frac{B}{T}\tau^2\right] \tag{4}$$

After demodulation, the baseband received radar echo signal can be formulated by a 2-D function as

$$s(t,\tau)=G(t)m\left(\tau-\frac{2r(t)}{c}\right)\exp\left[\mathrm{j}\pi\frac{B}{T}\left(\tau-\frac{2r(t)}{c}\right)^2\right]\exp\left[-\mathrm{j}\frac{4\pi}{\lambda}r(t)\right] \quad (5)$$

where

$\tau\in[-\frac{T}{2},\frac{T}{2}]$ is the range fast time, T is pulse duration, t is the azimuth slow time, c is the light speed, $G(t)$ is the beam pattern, $m(\tau)=\mathrm{rect}(\frac{\tau}{T})$. After range compression, the signal is

$$s(t,\tau)=G(t)\sin c\left[\pi B\left(\tau-\frac{2r(t)}{c}\right)\right]\exp\left[-\mathrm{j}\frac{4\pi}{\lambda}r(t)\right] \quad (6)$$

$r(t)$ consists of two part, the first part r_o is the distance of radar APC and turntable center after motion compensation, which is constant and has no effect on the imaging. $r_p(t)$ is the rotational component, and also is very important for the imaging. But in the forward squint imaging mode, r_o is the instantaneous distance of radar APC and imaging center, which can be expressed as $r_o(t)$. (x_p, y_p) is the distance of objective point related to imaging center, which doesn't change over time and has nothing to do with the airborne movement. $r_o(t)$ is translation component of the radar APC related to imaging area center. Eq. (6) can be expressed:

$$s(t,\tau)=G(t)\sin c\left\{\pi B\left[\tau-\frac{2(r_o(t)+r_p(t))}{c}\right]\right\}\times \exp\left[-\mathrm{j}\frac{4\pi}{\lambda}(r_o(t)+r_p(t))\right] \quad (7)$$

So the signal after range compression and motion compensation as

$$s(t,\tau)=G(t)\sin c\left\{\pi B\left[\tau-\frac{r_p(t))}{c}\right]\right\}\exp\left[-\mathrm{j}\frac{4\pi}{\lambda}r_p(t)\right] \quad (8)$$

Finally, focused image is made.

The maximum radius of imaging region is limited as $r_{\max}<\frac{2\rho^2}{\lambda}$, ρ is the image resolution. The LRD algorithm can get fine focused image, which provides a guarantee for the geometric distortion correction.

2.3 Geometric distortion correction

Due to the aforementioned geometric distortions, the following mosaicing processing is often unfeasible. The geometric distortion correction has to be carried out on the basis of point-by-point (Li *et al*., 2009; Ausherman & Kozma, 1984; Franceschetti & Perna, 2006a, 2006b). In Fig.5, we can see the imaging after geometric distortion correction for different squint angles. From Fig.6, the procedure about geometric distortion correction is described specifically as follows:

Step 1: The correction grid is firstly set in *XOY* paralleled to the *X* and *Y* axis. The sampling interval of neighboring correction points is $\Delta x=P_X$ and $\Delta y=P_Y$, where P_X and P_Y are equal to the 2-D pixel spacing in the resultant image.

Step 2: Calculate the 2-D position for each correction point in the subimage

Step 3: 2-D interpolation is employed in the real subimage domain to finish the correction. Fortunately, the removal of

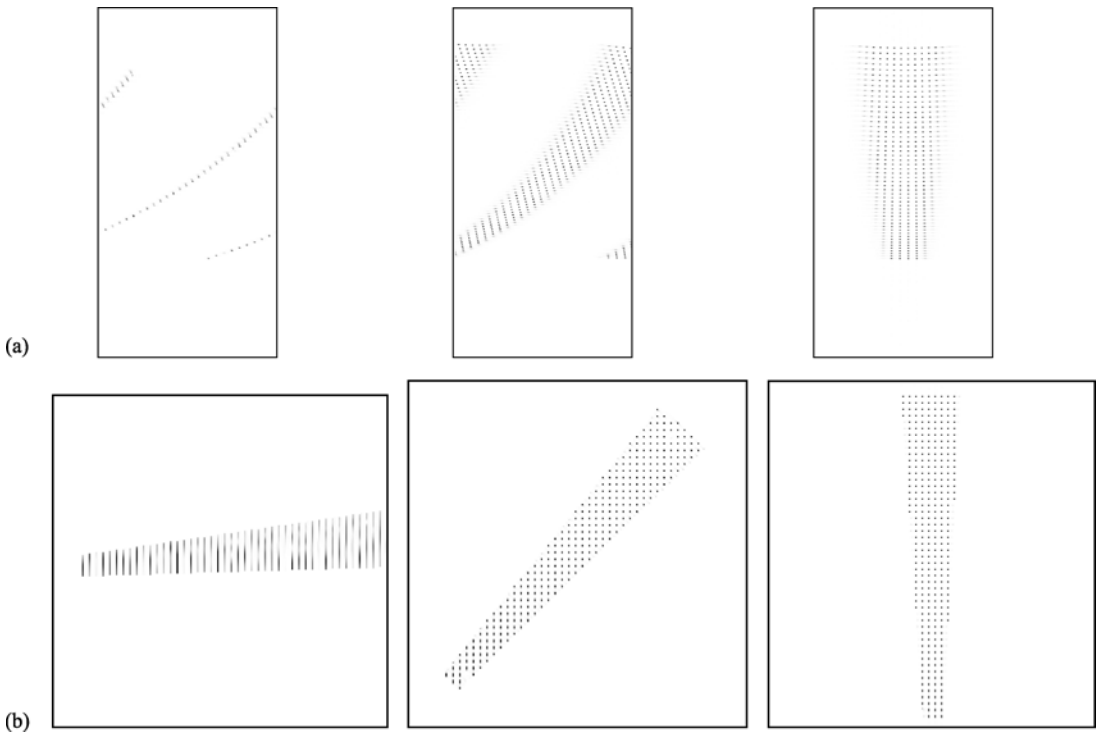

Fig. 5 Imaging after geometric distortion correction for different squint angles
(a) Before the geometric distortion correction; (b) After the geometric distortion correction
(The squint angles correspond for 85°, 46° and 2°, respectively.)

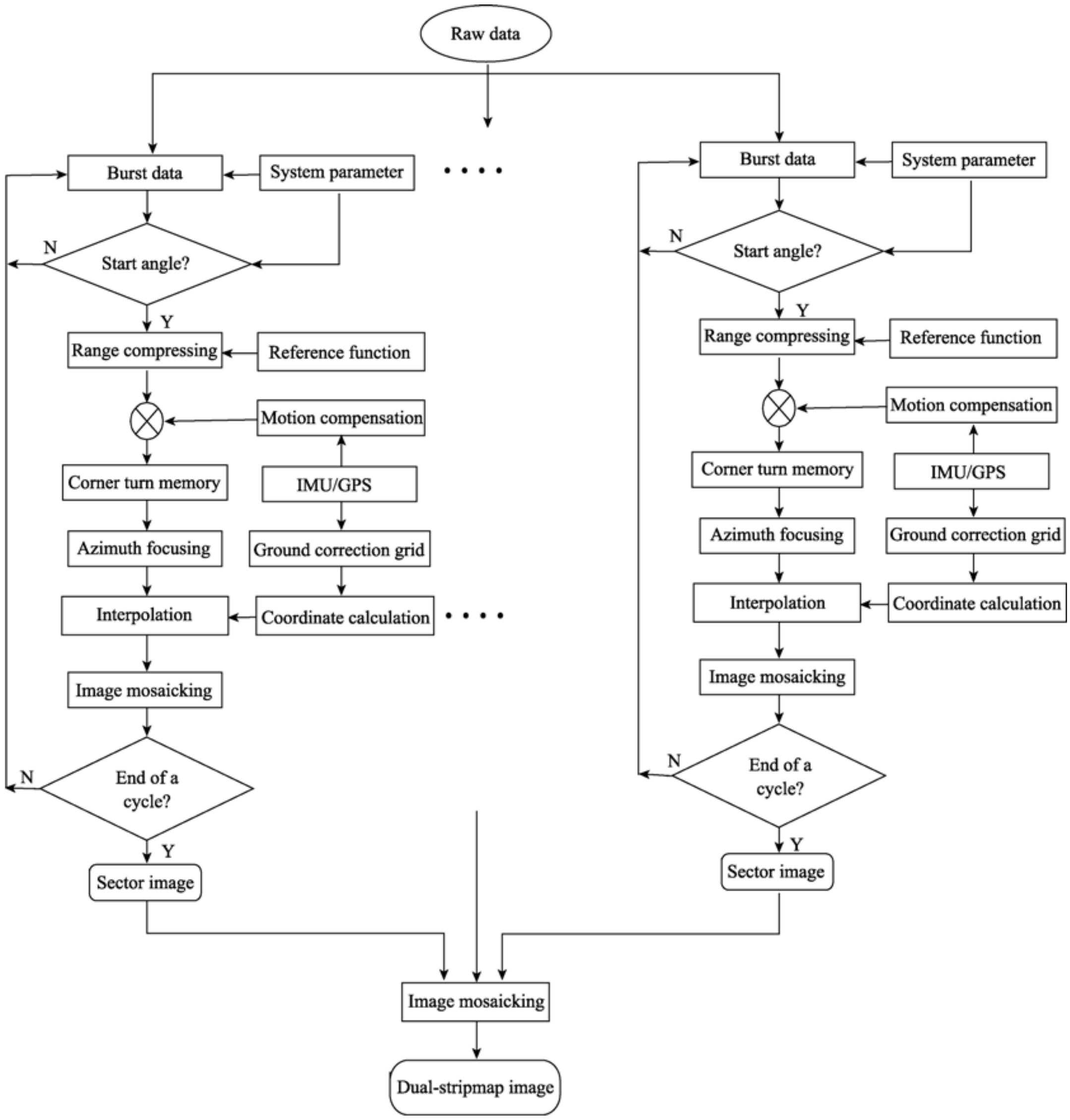

Fig. 6 Signal processing flowchart of the proposed system

phase term effectively reduces the computation burden.

3 DESIGN OF SYSTEM PARAMETER

The dual stripmap image aforementioned is obtained through a high-quality seamless mosaicing processing. To achieve this aim, the system parameters designment must be considered. The image resolution is firstly analyzed, because it is one of the most important system parameters. Then, other system performance parameters are discussed.

3.1 Range resolution and azimuth resolution

Since the sector image in the dual stripmap mode is mosaicked by many subimages, the resolution of subimage determines the resolution of sector image.

The radar transmits linear frequency modulation signal and realizes high resolution by pulse compression. The range resolution of subimage depends on the signal bandwidth, that is

$$\rho_r = \frac{c}{2B} \tag{9}$$

where c is velocity of light and B is the signal bandwidth.

It has been presented that the spotlight SAR image formation process can be beneficially extended to the stripmap mode followed with image mosaicing. So the azimuth resolution depends on the corner and squint angle from Eq. (10) and Eq. (11). The relationship of subimage azimuth resolution and squint angle is expressed in Fig.7. According to Fig.7, θ closes to 0°, the azimuth resolution is good, and vice versa.

$$\rho_a = \frac{\lambda}{2\Delta\theta\cos\theta_s} \tag{10}$$

and

$$\begin{cases} \Delta\theta = \dfrac{v_x \sin\varepsilon}{|CO|} T_{\text{sub}} \\ \varepsilon = \arccos\dfrac{\boldsymbol{v}_x \cdot \boldsymbol{CO}}{|\boldsymbol{v}_x| \times |\boldsymbol{CO}|} \end{cases} \tag{11}$$

where

λ is the wavelength;

θ_s is the squint angle;

$\Delta\theta$ is the angle through which the target is viewed during the coherent processing;

v_x is the velocity of the platform;

$|CO|$ is the distance between the APC and the imaging scene center;

$T_{\rm sub}=\dfrac{N_{\rm sub}}{\rm PRF}$ is the sub-aperture time, $N_{\rm sub}$ is the number of the pulses in subimaging, PRF is pulse repetition rate;

Therefore, subimage azimuth resolution ranges from $\dfrac{\lambda}{2\Delta\theta}$ to $\dfrac{\lambda}{2\Delta\theta\cos\theta_{\max}}$, $\theta_{\max}$ is the maximum squint angle of sector imaging area relative to airborne platform.

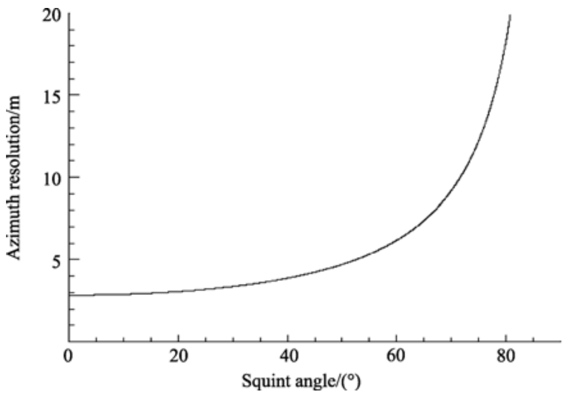

Fig. 7 Relationship curve of azimuth resolution angle

3.2 Antenna scanning speed and effective scanning angle

Effective angle is the central angle of sector imaging region in circular-scanning mode. If system parameters are designed illogically, the dual stripmap image will be discontinuous. On the one hand, the rotation rate and effective angle should be designed according with the resolution requirement to realize the seamless mosaicing between subimages.

If the dual stripmap image does not have the scene interrupt, radar movement distance L_s in a circular-scanning time should not be longer than the length of the imaging area S. When L_s equals to S, the repeated part in a dual stripmap image mosaicked by two sector images is the smallest. S should be the maximum distance between the X coordinate of the lower limit radius of sector imaging region. $[x_{r1}(t), y_{r1}(t), 0]$ is the 3-D position of ground projection of the lower limit radius.

$$\begin{cases} x_{r1}(t)=x(t)+r_1(t)\cos\theta_r(t) \\ y_{r1}(t)=y(t)+r_1(t)\sin\theta_r(t) \end{cases} \tag{12}$$

In Fig.8, S=x_b–x_a, S=$v(t_b$–$t_a)$+$2_{r1}\cos\alpha$, L_s=v_xT, $t_b-t_a=T\times\dfrac{\theta}{180^\circ}$.

If the stripmap images have non-mosaicing gap, the following condition should be met:

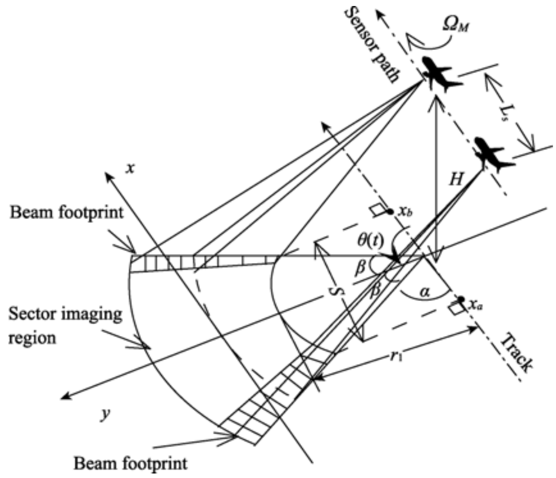

Fig. 8 Formation of imaging region according to and squint the system parameters

$$r_1\sin\beta \geqslant v_x\times\frac{180^\circ-\beta}{\Omega_M} \tag{13}$$

4 SIMULATION AND LIVE DATA PROCESSING RESULTS

In this part, to validate this new image mode, simulation results were given in Fig. 9. The main simulation parameters are listed in Table 1. Real data processing results and optical image that are taken from the same scene also evaluate the performance of dual stripmap imaging algorithm. Fig.10 shows some subimages before the image mosaicing.

Fig. 11 is the processing result of real data collected by an airborne circular-scanning SAR system. Fig.12 is the optical image of the same area. The Fig.9 and Fig.11 have correct geometric distribution, non-mosaicing slit and natural imaging transition. Comparing the two images, it can be concluded that the image formation algorithm can be used for general dual stripmap constellations and offers the high performance for the mosaicing procedure.

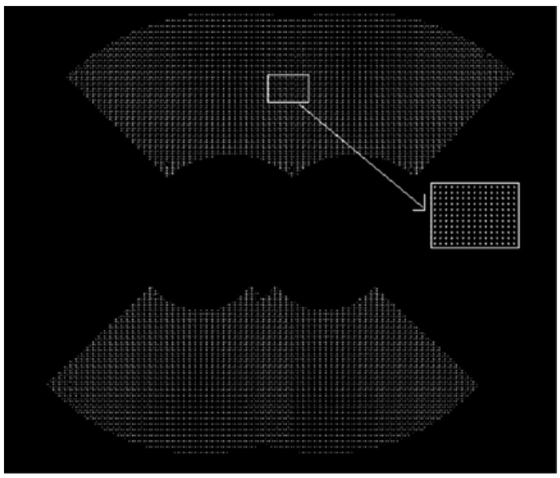

Fig. 9 Point objectives simulation result

Table 1 System parameters

Parameter	Value
Center frequency	X band
Imaging height	5000m
Azimuth beamwidth	3.8°
Range beamwidth	20°
Signal bandwidth	60MHz
Sensor velocity	140m/s
PRF	3000Hz
Antenna rotation rate	50°/s
Effective angle	60°
Image resolution	3m×3m

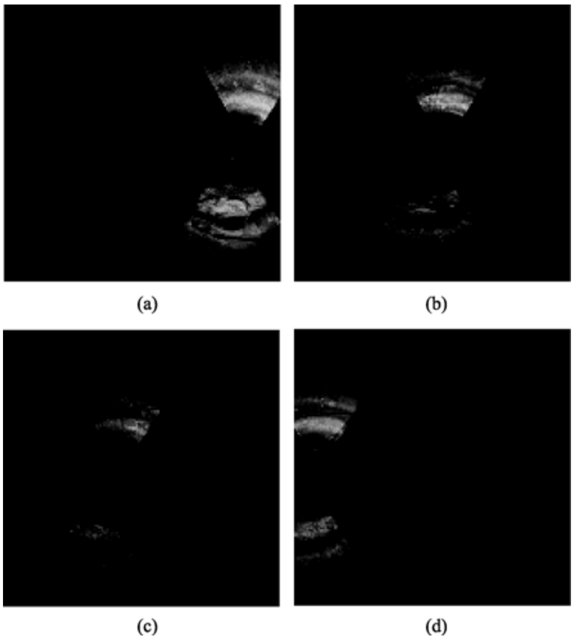

Fig. 10 Sector image of live data before image mosaicing

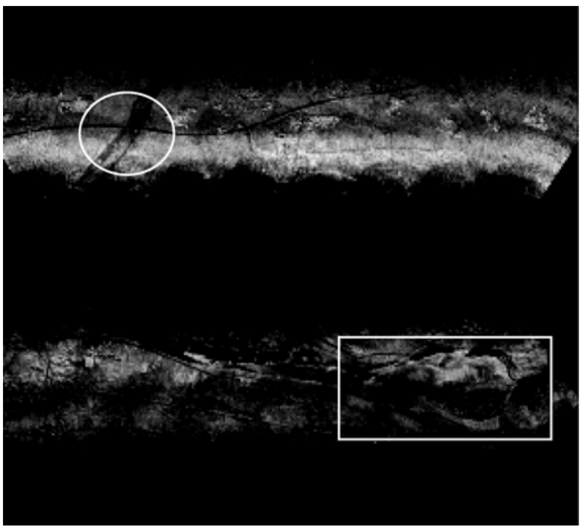

Fig. 11 Imaging processing result of the live SAR data

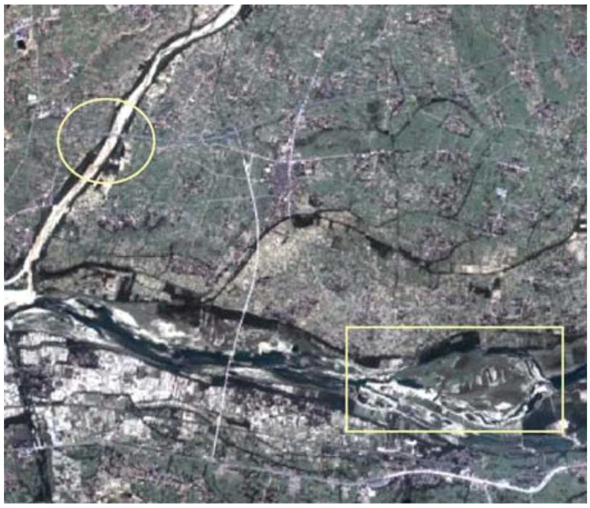

Fig. 12 Optical image of the same area

5 CONCLUSION

The dual stripmap imaging mode is based on circular scanning imaging mode, which is a newly developed imaging mode. It has complex process flow. According to the system parameters proposed by this paper, the dual stripmap image is obtained by mosaicing sector images after geometric distortion correction. An evaluation using point-target simulation and the processing results of live SAR data are provided. Their performances successfully demonstrate the validity of the proposed method.

REFERENCES

Ausherman D A and Kozma A.1984. Developments in radar imaging. *IEEE Trans.Aerosp. Electron. Syst*., **20**(4): 363—399

Carrara W G and Goodman R S. 1995. Spotlight Synthetic Aperture Radar Signal Processing Algorithms. New York :Artech House

Franceschetti G and Perna S.2006. SAR sensor trajectory deviations: Fourier domain formulation and extended scene simulation of Raw signal. *IEEE Transactions on Geoscience and Remote Sensing*. **44**(9): 33—39

Franceschetti G and Perna S. 2006. Efficient simulation of airborne SAR raw data of extended scenes. *IEEE Transactions on Geoscience Sensing*, **44**(10): 45—48

Ian G C and Frank H W. 2007. Digital Processing of Synthetic Aperture Radar Data: Algorithms and Implementation. Beijing: Publishing House of Electronics Industry

Li T C, Zhou Y Q and Cai S X. 2002. Study on the processing methods Bostoh Artech House for airborne circular scanning imaging radar. *Systems Engineer and Electronics*, **24**(7): 1—3

Li Y, Zhu D Y and Wang L. 2008. Study on the geometric distortion correction algorithm for circular-scanning imaging. IEEE International Geoscience & Remote Sensing Symposium, July 6—11 Bostoh Artech House

Li Y, Zhu D Y and Zhu Z D.2009.Geometric distortion correction algorithm for circular-scanning SAR imaging. *Journal of Nanjing University of Aeronautics and Astronautics*, **41**(2): 232—237

Mao X H, Zhu D Y, Li Y and Zhu Z D.2008. Study on error analysis of geometric distortion correction and compensation techniques for circular-scan SAR. *Journal of Electronics and Information Technology*, **30**(11): 37—43

Walker J L. 2007. Range-doppler imaging of rotation objects. *IEEE Transaction on Signal Processing*, **55**(3): 1011—1023

Zhu D Y and Zhu Z D.2005.Study on patch mapping by azimuth scan SAR. *Acta Aeronautica et Astronautica Sinica*, **26**(2): 208—213

环视 SAR 双条带成像实现方案

金雪松, 李　勇

南京航空航天大学 信息科学与技术学院 江苏 南京 210016

摘　要: 研究了一种双条带成像处理方案。该模式是对环视成像模式的扩展, 有效地提高了图像场景范围和成像处理效率。分析了双条带 SAR 成像处理的基本流程, 针对雷达运动平台的实际运动情况, 提出了一种满足图像分辨率和无缝拼接要求的系统实现方案以及相关系统参数的优化设计准则。借助点目标仿真和某型机载环视 SAR 外场试飞实测数据对该成像处理方案的有效性进行了充分地验证处理。

关键词: 合成孔径雷达, 双条带模式, 成像算法, 参数设计

中图分类号: TP722.6　　　**文献标识码:** A

引用格式: 金雪松, 李　勇. 2010. 环视 SAR 双条带成像实现方案. 遥感学报, **14**(4): 681—693

Jin X S and Li Y. 2010. Implementation of dual stripmap imaging for a novel airborne SAR system. *Journal of Remote Sensing*. **14**(4): 681—693

1 引　言

合成孔径雷达(SAR)具有全天候、全天时、远距离的成像能力, 广泛应用于地表测绘、资源勘探等领域。实现多种模式的高分辨率成像是 SAR 的发展方向之一, 经典的条带、聚束和扫描模式, 其成像带均位于雷达飞行路线的一侧; 环视模式 SAR(Li 等, 2008; 李天池等, 2002)(图 1)通过雷达天线以垂直方向为轴线的圆锥扫描不断获取机身 360°范围内散射体的雷达回波, 采用信号处理方法得到飞行路线下方环形区域的聚焦式 SAR 图像, 成像范围覆盖了载机航迹的两侧区域。然而, 聚焦型的环视 SAR 系统也有无法克服的缺陷。首先, 随着雷达波束的瞬时扫描, 天线指向的斜视角度不断增大, 导致合成孔径的利用率不断降低, 在雷达平台运动速度恒定的情况下图像的方位向分辨率会显著恶化; 其次, 当雷达波束指向载机运动的正前方和正后方时, 由于距离向和方位向信号完全耦合导致无法成像(毛新华等, 2008)。因此, 环视 SAR 图像的有效信息主要集中在左右两侧的正侧视区域, 而在大斜视和载机正前、正后方向区域的聚焦处理, 不仅耗费了硬件资源和运算时间, 且无法获取满意的成像结果。

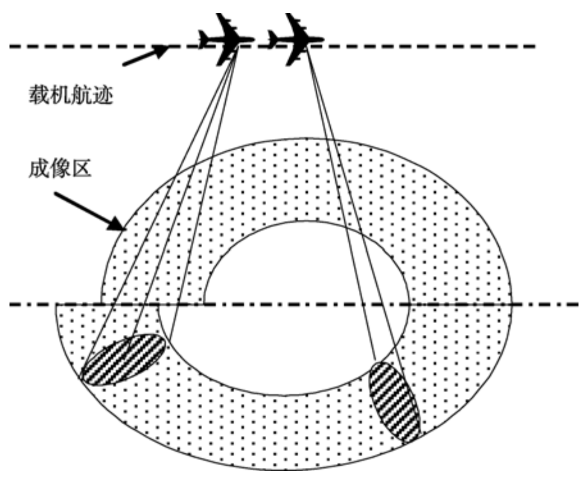

图 1　环视模式示意图

本文研究了一种可对雷达平台运动轨迹两侧区域同时进行条带测绘的 SAR 成像处理方法, 即双条带模式成像算法(图 2)。该工作模式是建立在环视 SAR 系统的基础上, 兼顾了大成像区域和高分辨率的成像要求, 以双正侧视附近区域的环视 SAR 图像为基础, 通过必需的几何校正及图像拼接处理获得了其他系统无法实现的能力。该模式弥补了单条带 SAR 图像在特殊领域应用上的不足, 可以与环视 SAR 结合提高各种航空兵器的匹配制导精度。文中分析了利用环视 SAR 系统实现双条带 SAR 成像的具体步骤并提出了该成像模式必需考虑的系统参数

收稿日期: 2009-06-05; 修订日期: 2009-11-03

基金项目: 航空科学基金(编号: 20080152004)和教育部博士点基金(编号: 20070287053)。

第一作者简介: 金雪松, (1985—　), 男, 安徽东至人, 硕士研究生, 研究方向: 雷达信号处理, E-mail: xuesong.jin@163.com。

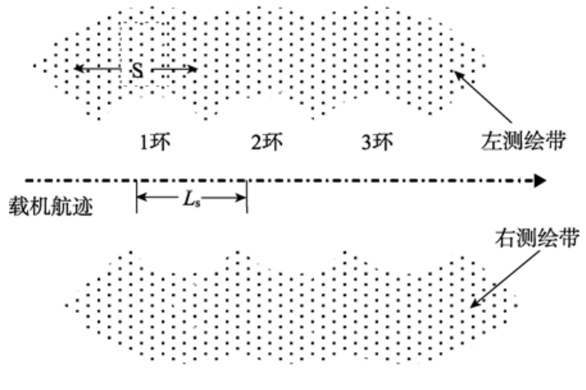

图 2 双条带 SAR 工作模式示意图

设计要求，通过点目标仿真和实测数据成像结果验证了该算法的有效性。

2 双条带 SAR 成像算法分析

双条带 SAR 成像算法的信号处理流程图如图3。雷达平台运动时天线波束以垂直地面方向为轴连续进行圆锥扫描并获取地物回波，对飞行路线左右正侧视区域回波进行成像处理；经几何失真校正后，将子块图像拼接成扇形图像；随着扇形图像不断产生、拼接，得到测绘区域的双条带图像。

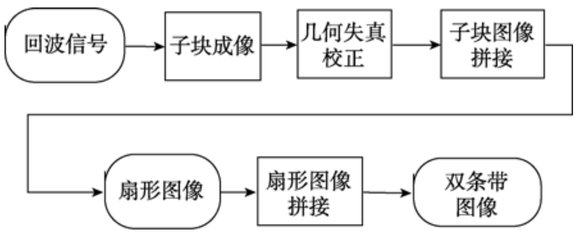

图 3 双条带 SAR 成像处理框图

2.1 成像模型分析

机载环视 SAR 系统的成像几何如图 4，以地面航迹方向为 x 轴正方向，垂直于地面航迹方向为 y 轴建立 XOY 坐标系，以地面波束足印描述 SAR 空间几何关系。$[x(t), y(t), H]$为飞机的坐标，H 是载机飞行高度，v_x 分别为飞机水平飞行速度，雷达载体的运动可由下面的参数方程描述

$$\begin{cases} x(t) = x(0) - v_x t \\ y(t) = y(0) \\ z(t) = H \end{cases} \tag{1}$$

式中，$[x(t), y(t), z(t)]$为时刻雷达载体的瞬时坐标，$[x(0), y(0), H]$为 t=0 即起始时刻雷达载体坐标。r_1、r_0 和 r_2 为波束足印内径、中心半径和外径，ϕ为下视

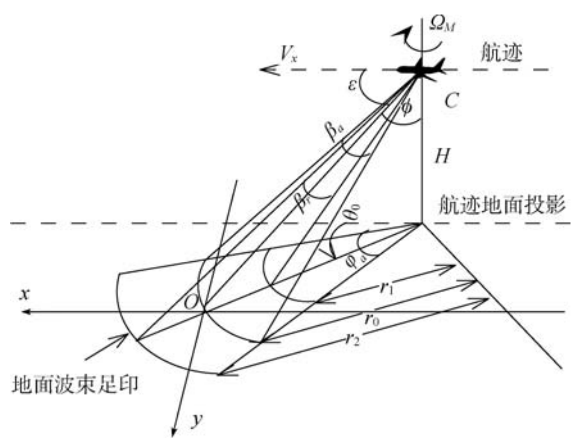

图 4 环视 SAR 系统成像的几何关系

角即雷达波束指向与高度方向夹角，β_a、β_r 分别为雷达波束方位和俯仰宽度，θ_0 为起始扫描角，Ω_M 为雷达波束扫描角速度，ε为雷达波束指向的空间斜视角，φ_a 为地面波束足印(图中阴影区域)对应的圆心角，可知

$$\begin{cases} r_0 = H\tan\phi \\ r_1 = H\tan\left(\phi - \dfrac{\beta_r}{2}\right) \\ r_2 = H\tan\left(\phi + \dfrac{\beta_r}{2}\right) \\ \varphi_a \approx \dfrac{\beta_a}{\sin\phi} \end{cases} \tag{2}$$

由(2)式可以确定雷达波束地面足印区域的大小，同时可知，φ_a 仅决定于方位波束宽度和下视角大小，与雷达载体飞行高度无关。地面波束足印中心坐标$[x_{of}(t), y_{of}(t), z_{of}(t)]$为

$$\begin{cases} x_{of}(t) = x(t) + r_0\cos\theta(t) \\ y_{of}(t) = y(t) + r_0\sin\theta(t) \\ z_{of}(t) = 0 \end{cases} \tag{3}$$

式中，$\theta(t)=\theta_0-\Omega_M t$ 表示 t 时刻雷达波束天线瞬时角度。

2.2 子块成像

子块成像应采用能在斜视情况下成像的SAR算法，本文采用了线性距离多普勒(LRD)算法(Walker, 2007；朱岱寅 & 朱兆达, 2005), LRD 算法是一种原理上基于转台成像的 SAR 成像算法，不仅满足 SAR 系统在大机动、大斜视条件下成像，而且计算量小、实时性好，适合工程应用。

载机飞行时，雷达波束的指向随时间进行旋转扫描，发射信号形式为

$$p(\tau) = m(\tau)\cos\left[2\pi\frac{c}{\lambda}\tau + \pi\frac{B}{T}\tau^2\right] \tag{4}$$

式(4)中，$\tau\in\left[-\dfrac{T}{2}, \dfrac{T}{2}\right]$为距离向的时间变量，$\lambda$为波长，

$m(\tau)$为发射信号包络, T 为脉冲宽度。则回波信号经过正交解调和脉冲压缩后表示为

$$s(t,\tau)=G(t)\sin c\left[\pi B\left(\tau-\frac{2r(t)}{c}\right)\right]\exp\left[-\mathrm{j}\frac{4\pi}{\lambda}r(t)\right] \quad (5)$$

式中, t 为方位向时间变量, $G(t)$代表天线对回波信号的加权, 发射信号包络 $m(\tau)$为矩形。经距离压缩后信号为:

$$s(t,\tau)=G(t)\sin c\left[\pi B\left(\tau-\frac{2r(t)}{c}\right)\right]\exp\left[-\mathrm{j}\frac{4\pi}{\lambda}r(t)\right] \quad (6)$$

式中, $r(t)$可分解为两个构造部分, 即 $r(t)=r_o(t)+r_p(t)$, 第一项 r_o 是经过运动补偿后雷达 APC 至转台中心的距离, 为一常数, 对成像无影响; $r_p(t)$表示目标相对于转台中心的转动分量, 它所引起的相位变化对成像是有用的, 正是 SAR 成像的依据所在。然而, 在前斜视成像模式中, 载机沿水平直线匀速飞行, r_o 代表的雷达 APC 与成像区中心的距离是瞬时变化的, 可以将其写为 $r_o(t)$。

$$s(t,\tau)=G(t)\sin c\left\{\pi B\left[\tau-\frac{2(r_o(t)+r_p(t))}{c}\right]\right\}\times \exp\left[-\mathrm{j}\frac{4\pi}{\lambda}(r_o(t)+r_p(t))\right] \quad (7)$$

式中, $r_o(t)$是需要补偿的平动分量, 它使得 $\sin c\{\cdot\}$在 τ轴上移动了 $\frac{2r_o(t)}{c}$, 同时距离向脉压后的信号相位变化了 $-\mathrm{j}\frac{4\pi}{\lambda}r_o(t)$。所以脉压后的信号经过距离对准和相位补偿后,

$$s(t,\tau)=G(t)\sin c\left\{\pi B\left[\tau-\frac{r_p(t))}{c}\right]\right\}\exp\left[-\mathrm{j}\frac{4\pi}{\lambda}r_p(t)\right] \quad (8)$$

最后进行方位聚焦成像。

LRD 算法对成像区域最大半径限制为 $r_{\max}<2\rho^2/\lambda$, ρ为图像分辨率。在给定分辨率和波长的条件下, 若目标距离成像区中心的半径小于 $r_{\max}$, 则采用该算法可以得到完全聚焦的 SAR 图像。考虑 SAR 系统的设计参数, $r_{\max}$ 的取值通常有数千米至数十千米, 所以采用 LRD 算法得到的子图图像不会出现散焦现象, 为后续的几何失真校正步骤提供了保证。

2.3 几何失真校正与图像拼接

图 5(a)为几何失真校正前图像, (b)为对应几何失真校正后图像, 对应斜视角分别为 85°、46°和 2°。斜视角越大, 图像的扭曲程度越严重。斜视角为 85°时, 几何失真校正前图像方位向出现了“卷绕”, 这是由于脉冲重复频率小于此时的多普勒带宽导致的, 另外由于此时距离与多普勒信息完全耦合, 故校正结果只能得到距离像, 方位像无法分辨; 斜视角为 46°时, 图像扭曲程度也比较严重但各点目标聚焦效果良好, 校正后图像与真实点目标分布一致; 斜视角为 5°时, 各点聚焦效果良好, 几何失真较小。

由于图像几何形变程度受雷达波束视角、平台飞航高度、成像区大小及斜视角等诸多因素影响。无论采用何种 SAR 算法得到的成像子块均存在几何失真, 失真的程度随着斜视角和成像区增大而日益严重(Ausherman & Kozma, 1984), 无法满足图像精度的要求, 必须对子图成像结果进行几何失真校正。

完整的双条带图像必须通过几何失真校正和图像拼接得到, 具体实现步骤如下(Li 等, 2009):

(1) 根据已知的系统参数预先计算出波束扫描时所能覆盖的地面区域范围, 确定最终输出图像的

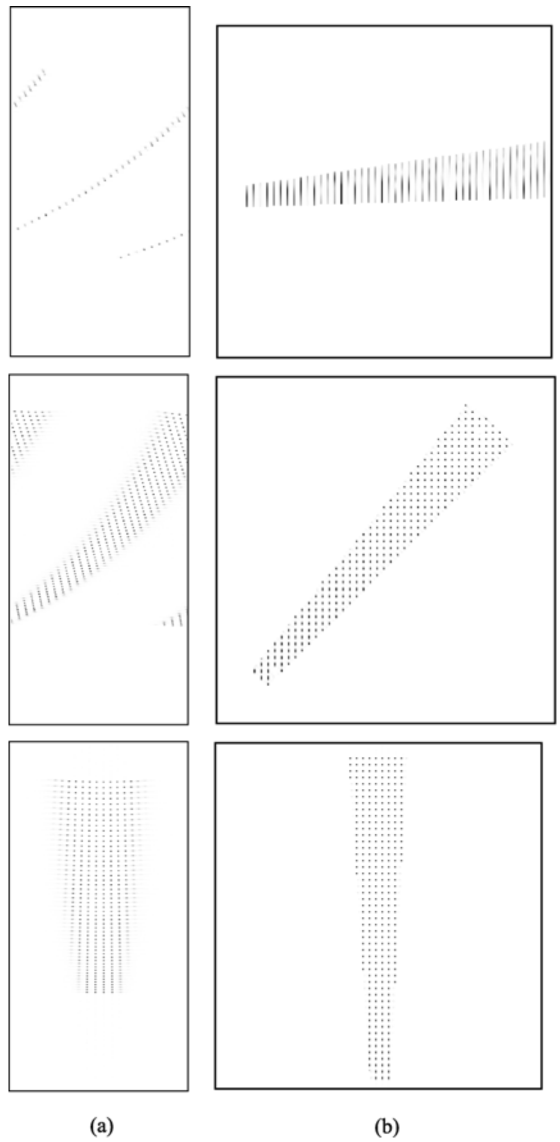

图 5 不同斜视角成像区域几何失真校正前后的图像
(a) 校正前; (b) 校正后
(斜视角分别对应为 85°、46°和 2°)

大小和像元点对应的地面校正网格点，各网格点间隔分别由方位向和距离向分辨率决定;

(2) 逐点计算当前成像区内各个地面校正网格点在成像结果中的位置;

(3) 通过插值将信号取出，放入(1)所确定的图像坐标系的二维数组中，完成几何失真校正;

(4) 随着成像子块图像得到校正、存储和输出，自动拼接成扇形图像;

(5) 第(4)步产生的扇形图像不断被输出，通过地理位置定标、赋形等相关处理后，最终拼接成双条带图像;

图 6 为双条带 SAR 信号处理流程图。

3 系统参数设计

双条带 SAR 的天线是不断进行圆锥扫描的，要得到无拼接缝隙高分辨双条带图像还要考虑系统参数设计问题。

3.1 距离向与方位向分辨率

由于双条带图像中的每个扇形图像是由若干个成像子块经过几何失真校正和拼接而成的，所以成像子块的分辨率决定着扇形图像的分辨率。

雷达发射线性调频信号，距离向进行脉冲压缩处理，成像子块的距离向分辨率取决于信号带宽，

$$\rho_r = \frac{c}{2B} \tag{9}$$

式中, c 是光速, B 为发射信号带宽。

本文所采用的子块成像思路是选取相邻波束足印的公共区域来等效为聚束照射，因此有较高的方位向分辨率，成像子块的方位向分辨率取决于载机相对于成像区域的总的转角大小和成像区中心对应

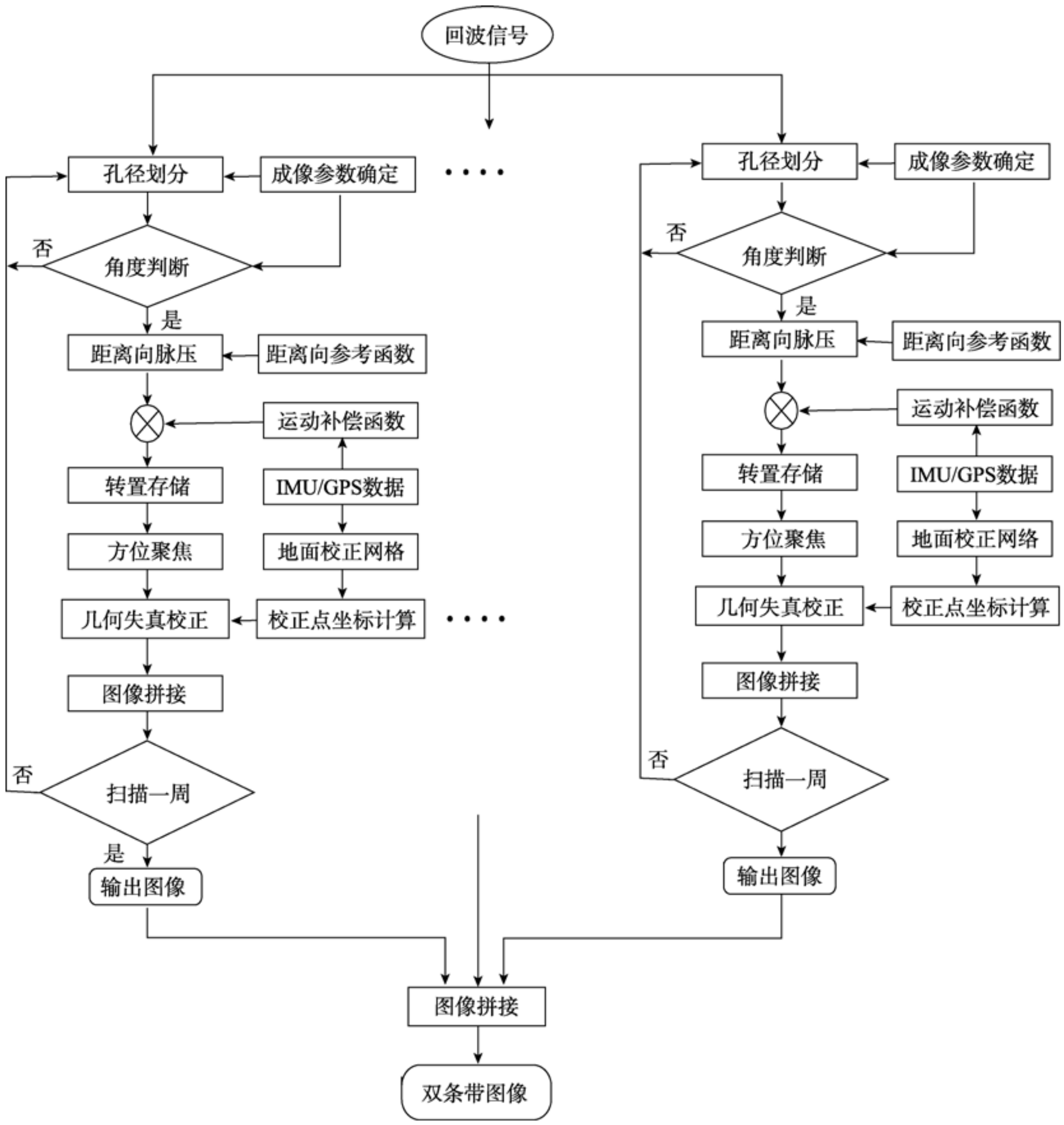

图 6 双条带 SAR 信号处理流程图

载机的斜视角，即

$$\rho_a = \frac{\lambda}{2\Delta\theta\cos\theta_s} \tag{10}$$

其中，

$$\begin{cases} \Delta\theta = \Omega T_{\text{sub}} \\ \Omega = \dfrac{v_x \sin\varepsilon}{|CO|} \\ \varepsilon = \arccos\dfrac{\boldsymbol{v}_x \cdot \boldsymbol{CO}}{|\boldsymbol{v}_x|\cdot|\boldsymbol{CO}|} \end{cases} \tag{11}$$

式中，θ_s 为斜视角即子孔径中心处天线波束中心与航线法向之间的夹角，$\Delta\theta$是载机相对于成像区域中心的总的转角，Ω为 SAR 平台相对于成像子块的等效旋转角速度，v_x 为 SAR 平台速度，ε为雷达波束指向的空间斜视角，$|CO|$为子孔径中心处载机与成像子块中心点的距离。$T_{\text{sub}} = \dfrac{N_{\text{sub}}}{\text{PRF}}$ 为子孔径时间，N_{sub} 为成像子块方位向积累脉冲个数，PRF 是脉冲重复频率。所以拼接扇形图像的成像子块方位向分辨率为 $\dfrac{\lambda}{2\Delta\theta}$ 到 $\dfrac{\lambda}{2\Delta\theta\cos\theta_{\max}}$ 之间，$\theta_{\max}$ 为扇形成像区域相对于载机的最大斜视角。

根据以上分析可知，成像子块方位向分辨率与斜视角关系如图 7，仿真中涉及参数见表 1。可见，在双条带成像模式中，越接近正侧视方向即θ越接近 0°的区域成像时方位向分辨率越高，斜视角越大，分辨率越低，但成像区域同时也越大。随着斜视角接近 90°时，即正前视或正后视方向，多普勒梯度几乎为零，距离向与方位向无法分辨，是环视成像的盲区。

3.2 天线扫描速度和有效扫描角度

有效扫描角度为扇形图像的中心角即单个环视扫描地面扇形成像区域的中心角，如图 8 中 2β角。由于雷达天线是进行圆锥扫描的，系统参数设计若

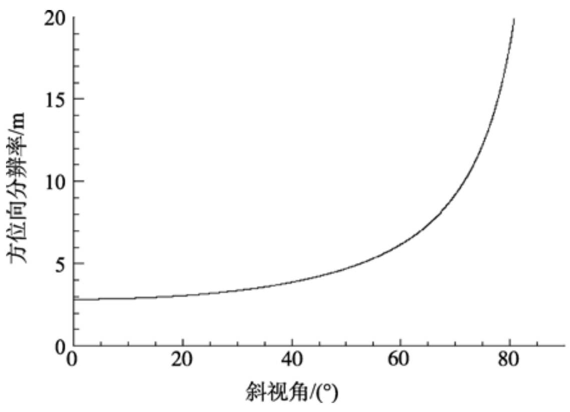

图 7 方位向分辨率与斜视角关系曲线

表 1 系统仿真参数

系统参数	取值
波段	X 波段
高度	5000m
方位波束宽度	3.8°
俯仰波束宽度	20°
LFM 信号带宽	60MHz
接收信号采样率	80MHz
载机速度	140m/s
脉冲重复频率	3000Hz
天线扫描角速度	50°/s
有效扫描角度	60°
图像分辨率	3m×3m

不合理，可能会出现存在场景中断的双条带 SAR 图像，所以天线扫描速度和有效扫描角度一方面要满足分辨率的要求，另一方面还要保证扇形图像能无缝拼接成双条带图像。如图 2 和图 8 双条带 SAR 图像若不存在场景中断，天线扫描一周的时间内载机飞行的距离 L_s 应小于等于该段时间内完成成像处理的地面区域长度 S，当 L_s=S 时，两个扇形图像的成像场景重复最小。S 应为地面扇形成像区域内径的 x 坐标之间的最大距离，约等于雷达天线扫描至扇形成像区域边缘的波束内径在地面投影的 x 坐标之间的距离，$[x_{r1}(t), y_{r1}(t), 0]$为波束内径在地面投影的坐标

$$\begin{cases} x_{r1}(t) = x(t) + r_1(t)\cos\theta(t) \\ y_{r1}(t) = y(t) + r_1(t)\sin\theta(t) \end{cases} \tag{12}$$

式中，$x(t)$、$y(t)$、$r_1(t)$、$\theta(t)$表述及计算方法见 2.1 节。图 8 中，S=x_b−x_a，x_a、x_b 为一个单侧扇形成像区域成像处理开始和结束时波束内径在地面的投影在 x 轴上坐标，故 S=$v(t_b-t_a)+2r_1\cos\alpha$，$L_s$=$v_xT$，$t_b-t_a$=$T\times\dfrac{\beta}{180^\circ}$，式中$\alpha$=90°−$\beta$。若所成双条带图像不存在场景间断，应满足条件：

$$r_1\sin\beta \geqslant v_x \times \frac{180^\circ-\beta}{\Omega_M} \tag{13}$$

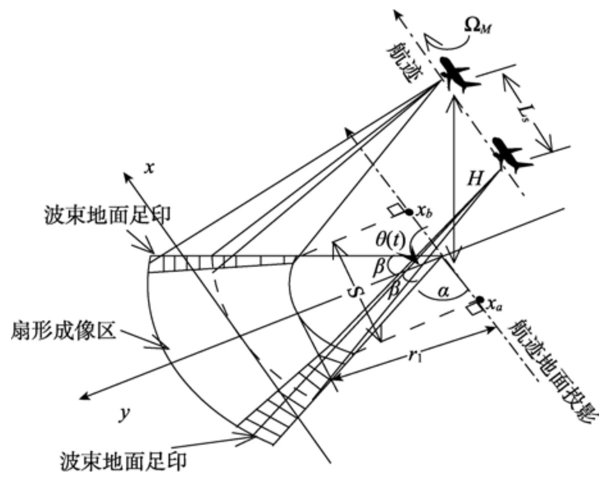

图 8 双条带 SAR 无缝拼接条件示意图

4 计算机仿真与实测数据验证

为验证双条带 SAR 成像算法的有效性，进行了点目标仿真研究，仿真参数见表 1。图 9 为仿真结果。图中双条带图像由两个扇形图像拼接而成，整个图像几何关系正确，无拼接缝隙，图像过渡自然，各点目标聚焦效果良好，经几何失真校正后排列整齐，清晰可辨。

图 10 是采用某型机载环视 SAR 系统录取的外场试飞实测数据处理的 SAR 图像。(a)、(b)、(c)、(d)是双条带 SAR 图像拼接之前部分扇形图像，是由若干完成几何失真校正的子图图像拼接而成；图 11 是拼接之后的双条带 SAR 图像，图中道路和河流场景连续、弯曲，无明显拼接缝隙，几何关系正确。与拼接之前单个环视SAR扇形成像相比，图11明显含有更多信息；与图 12 测绘地区光学图像比较，光学图像中的渡桥、立交桥、高速公路以及建筑物等重要地理目标在 SAR 图像对应位置处得以体现，可见图 11 如实反映了测绘区域的地理特征。

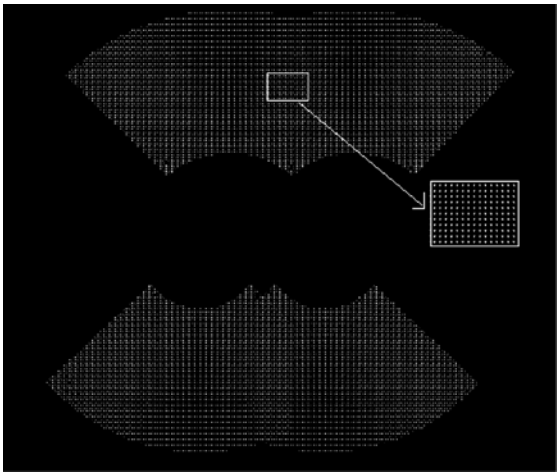

图 9 机载 SAR 双条带成像仿真

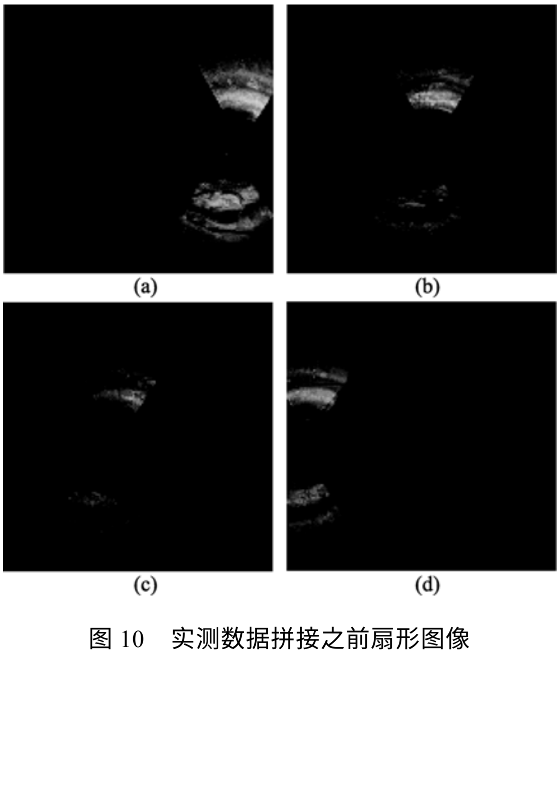

图 10 实测数据拼接之前扇形图像

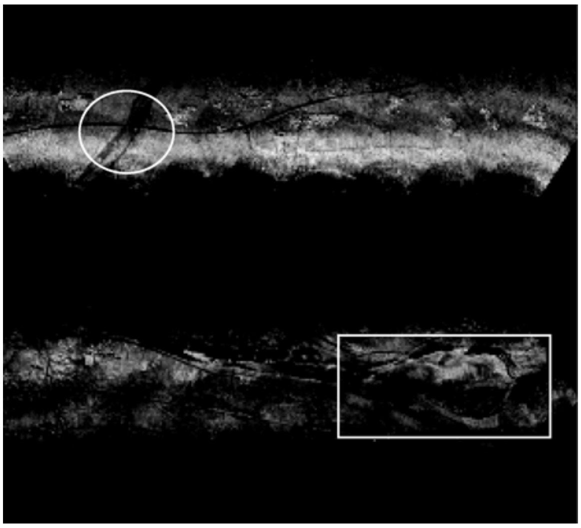

图 11 实测数据双条带 SAR 图像

图 12 同一地区的光学图像

5 结 论

机载 SAR 的双条带成像模式是建立在环视 SAR 基础上的、可对 SAR 平台两侧地面区域同时进行成像的一种新颖的工作模式，其成像处理的流程复杂，根据本文提出的系统参数设计方法对测绘区域进行环视扫描，经过子块成像处理、几何失真校正和图像拼接后能够得到无场景中断的双条带 SAR 图像。点目标仿真和实测数据成像处理的结果表明，本文研究的双条带 SAR 成像处理方法是正确有效的。

REFERENCES

Ausherman D A and Kozma A.1984. Developments in radar imaging. *IEEE Trans.Aerosp. Electron. Syst*., **20**(4): 363—399

Carrara W G and Goodman R S. 1995. Spotlight Synthetic Aperture Radar Signal Processing Algorithms. New York :Artech House

Franceschetti G and Perna S.2006. SAR sensor trajectory deviations: Fourier domain formulation and extended scene simulation of Raw signal. *IEEE Transactions on Geoscience and Remote Sensing*. **44**(9): 33—39

Franceschetti G and Perna S. 2006. Efficient simulation of airborne SAR raw data of extended scenes. *IEEE Transactions on Geoscience Sensing*, **44**(10): 45—48

Ian G C and Frank H W. 2007. Digital Processing of Synthetic Aperture Radar Data: Algorithms and Implementation. Beijing: Publishing House of Electronics Industry

Li T C, Zhou Y Q and Cai S X. 2002. Study on the processing methods Bostoh Artech House for airborne circular scanning imaging radar. *Systems Engineer and Electronics*, **24**(7): 1—3

Li Y, Zhu D Y and Wang L. 2008. Study on the geometric distortion correction algorithm for circular-scanning imaging. IEEE International Geoscience & Remote Sensing Symposium, July 6—11 Bostoh Artech House

Li Y, Zhu D Y and Zhu Z D.2009.Geometric distortion correction algorithm for circular-scanning SAR imaging. *Journal of Nanjing University of Aeronautics and Astronautics*, **41**(2): 232—237

Mao X H, Zhu D Y, Li Y and Zhu Z D.2008. Study on error analysis of geometric distortion correction and compensation techniques for circular-scan SAR. *Journal of Electronics and Information Technology*, **30**(11): 37—43

Walker J L. 2007. Range-doppler imaging of rotation objects. *IEEE Transaction on Signal Processing*, **55**(3): 1011—1023

Zhu D Y and Zhu Z D.2005.Study on patch mapping by azimuth scan SAR. *Acta Aeronautica et Astronautica Sinica*, **26**(2): 208—213

附中文参考文献

李天池，周荫清，蔡世学．2002．机载环扫雷达数据处理方法研究．系统工程与电子技术, **24**(7): 1—3

李勇，朱岱寅，朱兆达．2009．环视 SAR 成像处理中的几何失真校正算法．南京航空航天大学学报, **41**(2) : 232—237

毛新华，朱岱寅，李勇，朱兆达．2008．环视 SAR 几何失真校正误差分析及补偿技术研究．电子与信息学报, **30**(11): 37—43

朱岱寅，朱兆达. 2005．方位扫描 SAR 区域成像研究．航空学报, **26**(2): 208—213